Local photocurrent mapping as a probe of contact effects and charge carrier transport in semiconductor nanowire devices

Y. Gu, J. P. Romankiewicz, J. K. David, J. L. Lensch, and L. J. Lauhon[a]
Department of Materials Science and Engineering, Northwestern University, Evanston, Illinois 60208

E.-S. Kwak and T. W. Odom
Department of Chemistry, Northwestern University, Evanston, Illinois 60208

Three types of two-terminal CdS nanowire devices with distinct current versus voltage characteristics were fabricated by forming Schottky and/or Ohmic contacts in a controlled manner. Argon ion bombardment of CdS nanowires increased the carrier concentration allowing the formation of Ohmic Ti–CdS contacts. Scanning photocurrent microscopy (SPCM) was used to explore the influence of the contacts on the spatially resolved photoresponse in two-terminal devices and to analyze charge carrier transport processes. Modeling of the spatial profiles of the local photocurrent images enabled the quantitative extraction of electron and hole mobility-lifetime products in Ohmic devices and the hole mobility-lifetime product in Schottky devices. Analysis of the evolution of SPCM images with bias suggests that the electric field is localized to the optical generation region in the Ohmic devices and localized beneath the contacts in the Schottky devices. © *2006 American Vacuum Society.* [DOI: 10.1116/1.2216717]

I. INTRODUCTION

One-dimensional nanomaterials such as semiconductor nanowires and carbon nanotubes are being developed as building blocks for high performance electronic and photonic devices. The first step in the integration of these building blocks into circuits is the attachment of electrical contacts, the character of which is very sensitive to fabrication procedures and can greatly affect nanoscale device characteristics. In early work[1] on carbon nanotube field-effect transistors, for example, device characteristics that were dominated by contact effects delayed an eventual understanding of the device physics. To develop device technologies based on one-dimensional (1D) materials, it will be essential to be able to produce various types of electric contacts (Schottky and Ohmic) in a consistent and controlled manner, and to be able to directly verify the nature of the contacts. Characterization techniques that are sensitive to the nature of the contacts and are also capable of probing the carrier transport properties intrinsic to the semiconducting material are therefore desired.

Here we report the controlled fabrication of Schottky and Ohmic Ti–CdS electrical contacts to single CdS nanowires and the measurement of two-terminal device characteristics that are consistent with the nature of the contacts. Ohmic contacts were obtained on intrinsically *n*-type CdS nanowires subject to *in situ* Ar$^+$ bombardment followed by Ti contact evaporation, while the direct evaporation of Ti on HF-etched CdS nanowires resulted in Schottky contacts. Back-to-back Schottky-barrier devices, Schottky diodes, and Ohmically contacted devices were fabricated, and the expected current versus voltage (*I-V*) characteristics were consistently ob-

served. Scanning photocurrent microscopy[2,3] (SPCM) images exhibited localized responses that were used to confirm the nature of the contacts and to analyze carrier transport processes in these devices. Both near-field scanning optical microscopy (NSOM) and scanning confocal microscopy were employed in the local photocurrent measurements to obtain a spatial resolution much smaller than the nanowire device length. For Schottky-barrier devices, the electric field was found to be highly localized to the contact region as expected, and the photogenerated carriers diffuse from the nanowire channel region into the space-charge region (Schottky-barrier region), where they are collected. In contrast, both drift and diffusion occur in different portions of the channel region in Ohmic devices. This enabled quantitative measurements of the electron and hole mobility-lifetime products ($\mu\tau$), a quantity intrinsic to the nanowires and an important figure of merit for photodetectors[4,5] and photovoltaics.[6] For Schottky diodes, SPCM images and transport characteristics were similar to those of Schottky-barrier (Ohmic) devices under reverse (forward) bias.

II. EXPERIMENT

Single CdS nanowires (with average diameter of ∼60 nm) were synthesized via thermal chemical vapor deposition and gold-catalyzed vapor liquid solid growth using 50 nm gold colloids. The nanowires were dispersed in isopropanol and subsequently deposited on degenerately doped Si substrate capped with 400 nm SiO$_2$, followed by spin coating of methyl methacrylate (MMA) and poly(methyl methacrylate) (PMMA) layers. The contact areas were defined by e-beam lithography. Various two-terminal devices were fabricated following three types of fabrication procedures: in procedure A [Fig. 1(a)], both nanowire contact re-

---

[a]Author to whom correspondence should be addressed; electronic mail: lauhon@northwestern.edu
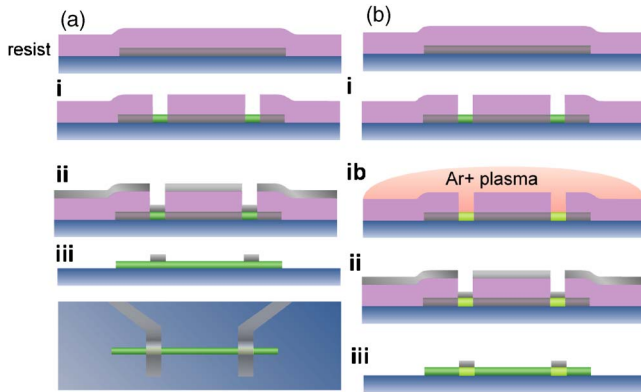
FIG. 1. Schematic of procedures A (a) and B (b) for fabricating Schottky and Ohmic contacts, respectively, on CdS nanowires. Contact regions are defined on resist-coated CdS nanowires by e-beam lithography (i). In (a), CdS nanowires are etched by HF before Ti metal evaporation (ii) followed by lift-off (iii). For procedure B (b), CdS nanowires are subject to Ar$^+$ bombardment (ib) followed by steps (ii) and (iii). The typical diameter of CdS nanowires is 60 nm and the electrode thickness is around 200 nm with a width of 1 μm. For clarity, the schematics shown here are not to scale.

gions were etched by HF before Ti evaporation and the lift-off; in procedure B [Fig. 1(b)], both contact regions were subject to *in situ* Ar$^+$ bombardment followed by Ti evaporation and the lift-off; in procedure C (not shown), one contact region was subject to *in situ* Ar+ bombardment and the other was etched by HF followed by Ti evaporation and the lift-off. A number of devices of each type were made, and all exhibited electrical characteristics typical of the group. For clarity, devices fabricated following procedure A (B or C) will be denoted as device A (B or C) throughout the rest of the article, unless otherwise noted.

I-V characteristics were measured using a Keithley semiconductor characterization system. Due to the intrinsic nature of the CdS nanowires, the dark current was extremely low (a few picoamperes or less), so weak background (room light) illumination was used to increase the conductivity of nanowire devices to obtain reliable measurements. The *I-V* characteristics were also measured under global illumination provided by a fiber lamp to provide a global photoconductivity reference for the local photoconductivity measurements.

The SPCM measurements were carried out using either a NSOM, where the local optical excitation is provided by a Ti: sapphire laser (λ=400 nm) coupled to an Al-coated optical fiber with diameter ~200 nm and an optical aperture ~70 nm, or a scanning confocal microscope (for devices B and C) with a high numerical aperture (NA=0.75) objective, from which an Ar+ laser (λ=457 nm) was focused to a diffraction-limited laser spot. The experimental schematic is shown in Fig. 3(a). The photocurrent, measured using a current preamplifier and lock-in detection with the laser chopped at 1–2 kHz, was recorded as a two-dimensional map as the optical fiber tip or the microscope objective was scanned across the nanowire device under study. Reflected
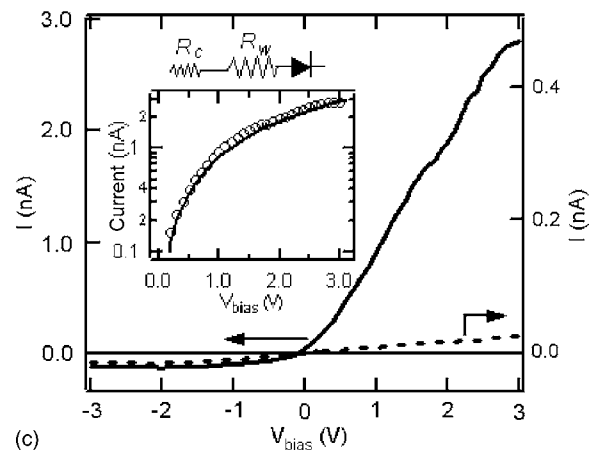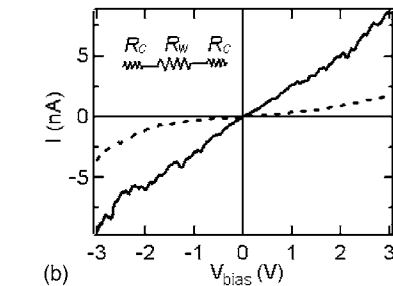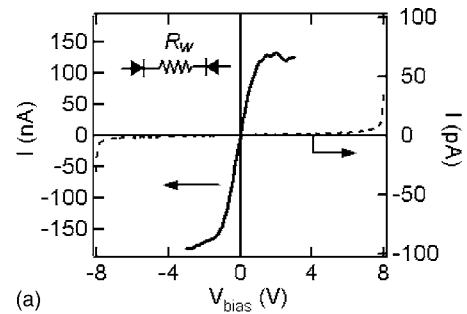
FIG. 2. Typical current-voltage (*I-V*) characteristics of (a) Schottky-barrier devices (device A), (b) Ohmic devices (device B), and (c) Schottky diodes (device C) under weak room light (dashed lines) and fiber lamp illumination (solid lines). R_c and R_w represent the contact resistance and the nanowire resistance, respectively. In the inset to (c), the *I-V* curve of the Schottky diode in (c) is plotted on a semilogarithmic scale (open circles) and fit (solid lines) to thermionic-diffusion theory.

light images were recorded simultaneously to determine the location of the contacts. All the measurements were carried out at room temperature.

III. EXPERIMENTAL RESULTS

Figures 2(a)–2(c) show the typical global *I-V* characteristics that have been consistently observed for devices fabricated following procedures A, B, and C, respectively. Under weak room light, device A showed very little current (<2 pA) with V_{bias}<7 V, beyond which a sudden increase in the current was observed, while under fiber lamp illumination the current was much higher and saturated at V_{bias} ~1.5 V. Device B, on the other hand, showed *I-V* characteristics that were linear under fiber lamp illumination and slightly nonlinear under weak room light, consistent with
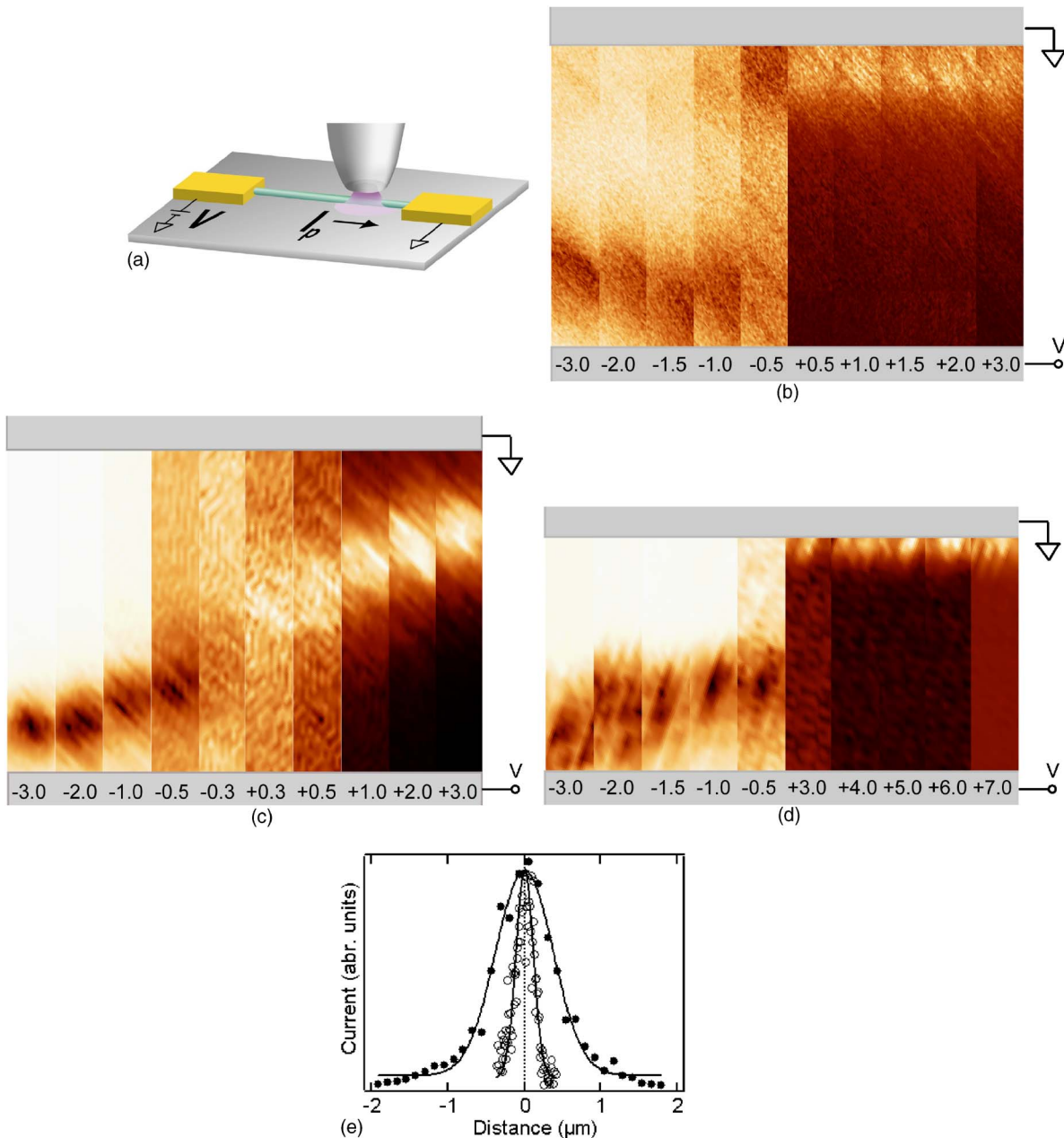
FIG. 3. (a) Schematic of SPCM setup. Photocurrent images of (b) a Schottky-barrier device (device A), (c) an Ohmic device (device B), and (d) a Schottky diode device (device C) under various biases. The channel lengths are 0.8, 5.8, and 2.5 μm, respectively. The normalized photocurrent profile perpendicular to the nanowire channel is plotted in (e) for the measurements using a near-field scanning microscope [open circles, from (b)] and a scanning confocal microscope [solid circles, from (c)] and is fit by Gaussian functions (solid lines).

space-charge-limited current. While both devices A and B exhibited symmetric *I-V* characteristics, device C showed highly asymmetric (rectifying) *I-V* characteristics both under weak room light and with fiber lamp illumination. The inset to Fig. 2(c) shows the fit to the *I-V* data from device C (semilog plot) using thermionic-diffusion theory.[7]

Figure 3 shows SPCM images of devices A, B, and C under various biases. A scanning confocal microscope was used for the measurements on devices B and C with channel lengths about 5.8 and 2.5 μm, respectively. A NSOM system (with higher spatial resolution, see below) was used for device A as this device had a shorter channel length (0.8 μm)

and the photocurrent was more localized; as discussed below, the resolution of NSOM was necessary to analyze the photocurrent profile. For all the images, a photocurrent peak was observed closer to the negatively biased electrode (hole collector). For device A [Fig. 3(b)], the photocurrent peak was strongly localized to the contact region and no significant spatial variations with bias were observed. The photocurrent images of device B [Fig. 3(c)], on the other hand, exhibited different characteristics as the photocurrent peak was not localized to the contacts and shifted continuously towards the negatively biased electrode with increasing bias. Device C [Fig. 3(d)] showed characteristics of devices A and B: the

photocurrent image characteristics resemble those from device A (B) when the bottom electrode was positively (negatively) biased. Similar image characteristics were consistently observed for other devices within each group. The resolution of SPCM images taken with NSOM and the confocal microscope was determined by analyzing line scans perpendicular to the device channel [Fig. 3(e)]. The widths estimated by Gaussian peak fitting correspond approximately to the sum of the nanowire diameter and the width of the light spot, which is 80 nm (470 nm) in the case of NSOM (scanning confocal microscope), consistent with the size of the optical aperture (diffraction-limited spot). The spatial profiles of the photocurrent along the nanowire channel are shown on a semilogarithmic scale in Figs. 4(a)–4(c) for devices A, B, and C, respectively. The solid lines are exponential fits to the profiles on either side of the peak and no significant difference is observed in the spatial extension of the photocurrent profile for a given device under various biases.

For greater insight into the common characteristics of devices of the same group but with different channel lengths, the fractional spatial shifts (ratio of the shift to the channel length) of the photocurrent peaks from devices B1 and B2 are plotted in Figs. 5(a) and 5(b) both as a function of the applied bias V_{bias} [Fig. 5(a)] and the electric field V_{bias}/L [Fig. 5(b)], where L is the device channel length. It is clear that the fractional spatial shift as a function of the bias shows similar behaviors for both devices, whereas the plot as a function of V_{bias}/L differs between these two devices.

IV. DISCUSSION

From Fig. 2, it is clear that the device characteristics are determined by the contact fabrication procedures. Indeed, a Schottky barrier forms between Ti and intrinsic CdS with a barrier height ~0.7 eV,[7] leading to the blocking *I-V* characteristics (very low current under weak room light) observed from device A (Schottky-barrier device) and the current saturation observed under global illumination, consistent with back-to-back Schottky diode photodetectors.[8] On the other hand, subjecting intrinsic CdS to *in situ* Ar⁺ bombardment significantly enhances the electric conductivity by introducing donor-type impurities,[9,10] narrowing the Schottky barrier and significantly increasing the tunneling current across the metal-semiconductor interface. The resulting *I-V* characteristics are Ohmic (linear) despite the use of the same contact metal in the type B devices. When these two types of contacts (A and B) are fabricated on either end of a nanowire, asymmetric (rectifying) *I-V* characteristics are expected and are indeed observed from device C, which is essentially a Schottky diode. Fitting the *I-V* curve using thermionic-diffusion theory yields a barrier height of ~0.4 eV, in reasonable agreement with the value of barrier height between Ti and the intrinsic CdS (0.7 eV), with an ideality factor around 4.

The nature of the contacts is further explored by the SPCM experiments, which reveal distinct carrier transport process associated with different types of contacts. The
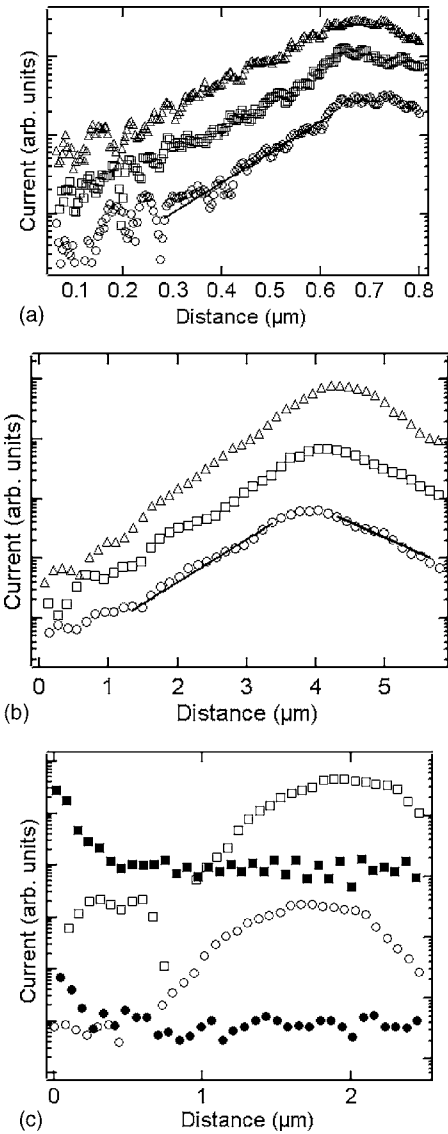
FIG. 4. Semilogarithmic plot of the photocurrent profiles of (a) the Schottky-barrier device (device A) under biases of 1 V (open circles), 2 V (open squares), and 3 V (open triangles); (b) the Ohmic device (device B) under biases of 1 V (open circles), 2 V (open squares), and 3 V (open triangles); and (c) the Schottky diode (device C) under forward biases of 0.5 V (open circles) and 3 V (open squares), and under reversed biases of 3 V (solid circles) and 5 V (solid squares). The profiles are offset along the *y* axis for clarity.

strong localization of photocurrent peak to the near-contact region, which is observed for device A under all biases and for device C at the reverse bias condition (where the Schottky contact is negatively biased), suggests a strong electric field in the contact region, characteristics of Schottky barriers. The carrier transport process in the nanowire channel region in this case is purely diffusive as only carriers within the distance equal to the diffusion length from the contact region can be collected, and this is confirmed by the absence of photocurrent outside of the contact region.[3] The appearance of photocurrent near the negatively bias contact (hole collector) indicates that the electron diffusion is much more efficient than hole diffusion, as discussed in detail in
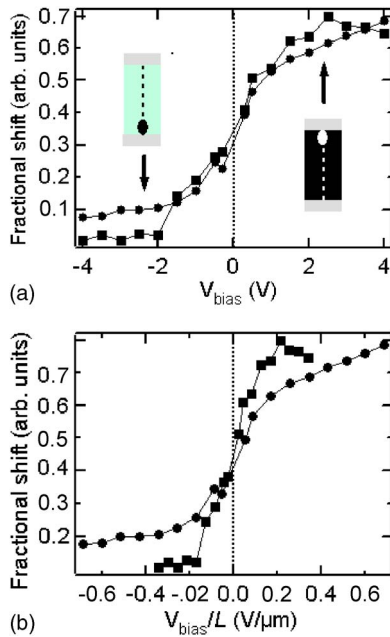
FIG. 5. Fractional photocurrent peak position as a function of (a) V_{bias} and (b) V_{bias}/L, where L is the device channel length, for device B1 (solid circles, $L=5.8$ μm) and device B2 (solid squares, $L=11$ μm).

Ref. 3. For device B, and device C under the forward bias condition, the photocurrent images show completely different characteristics as the photocurrent peak is not localized to the contact and the peak position continuously shifts towards the hole collector with increasing bias. This indicates that the electric field is not localized to the contact region, which is expected for Ohmic contacts. In this case, the photogenerated carriers are separated by the electric field in the middle of the nanowire; those carriers that reach the electrodes before recombining contribute to the photocurrent. The photocurrent peak appears closer to the negatively biased electrode (hole collector) at all biases, indicating that hole drift/diffusion is the limiting factor in the charge collection process. While increasing the bias enhances both electron and hole collection efficiencies, the higher electron mobility in CdS implies that the differential increase in the number of electrons collected is greater than that in the number of holes collected, as reflected in the continuous shift of the photocurrent peak towards the hole collector observed for device B, as well as device C under forward bias. We conclude that SPCM can unambiguously confirm the controlled formation of different types of contacts and that the proposed carrier transport processes are consistent with the nature of the contacts.

The sensitivity of SPCM images to carrier transport processes also allows one to gain quantitative insight into the carrier transport characteristics by fitting of the photocurrent profiles, as we recently reported.[11] Here we summarize the analysis, while highlighting the influence of and limitations posed by the contacts. The photocurrent profiles of device A [Fig. 4(a)] decay exponentially as the probe moves away from the hole collector. The decay length can be interpreted as the characteristic length that photoexcited holes travel be-

fore recombining. The slope of the profile is independent of bias, indicating that the space-charge region associated with the Schottky barrier lies beneath the electrode, and does not extend significantly into the nanowire channel region for the range of voltages studied. The characteristic length is therefore associated with the hole diffusion length ($L_h \sim 110$ nm), which was determined by the fitting to the photocurrent profile [Fig. 4(a)]. Using the relation $L_h=(D\tau)^{1/2}$, where D and τ are the carrier diffusion coefficient and the carrier lifetime, respectively, and the Einstein relation $\mu =(q/k_BT)D$, one can determine the hole mobility-lifetime product $\mu\tau$ as $(q/k_BT)L_h^2$, which is 0.47 μm/(V/μm). The mobility-lifetime product, which represents the average carrier drift length per unit electric field, is an indicator of charge carrier collection efficiency and is an important figure of merit for photodetectors and photovoltaics. While the strongly localized electric field in the Schottky-barrier devices allows the measurement of $\mu\tau$ for holes, the measurement of $\mu\tau$ for electrons is precluded because the photocurrent peak does not occur in the middle of the channel.

In the Ohmic device B [Fig. 4(b)], the peak in SPCM images occurs in the middle of the channel, indicating that the electric field is not localized to the contact regions. This allows analysis of the exponential photocurrent decay associated with both electron and hole limited currents. As required by the current continuity condition, the electron current flowing across the electron collector (left) must be equal to the hole current flowing across the hole collector (right), and this implies that the steady-state current is limited by the hole (electron) current when the optical excitation point moves away from the hole (electron) collector and towards the electron (hole) collector. The magnitude of the current is proportional to the number of carriers reaching the electrode, so the decay of the photocurrent profile towards the electron (hole) collector represents the hole (electron) concentration distribution, which varies exponentially with distance. Because one would expect that the electric field produced by the applied bias will modify the carrier distribution through drift processes, one would expect the photocurrent decay length to be field dependent, but the slopes are independent of bias within the resolution of the measurement. We believe this to be the effect of space charges induced by the local optical excitation. Qualitatively, the applied electric field is effectively confined within the space-charge region, and its effect is to separate the photogenerated electrons and holes, which then *diffuse* to the corresponding electrodes.[11] Although the validation of this picture will require theoretical modeling, it is supported by the data of Fig. 5 discussed below. From fits to the spatial extension of the electron and hole concentrations one can determine $\mu\tau$ to be 27 μm/(V μm) for electrons and 14 μm/(V μm) for holes. These values are significantly higher than those obtained from device A and they are also higher than typical bulk values [16 μm/(V μm) for electrons[12] and 6 μm/(V μm) for holes[13]]. The carrier mobility in these nanowires is not likely to be higher than bulk because of the effects of surface scattering, so we conclude that the carrier recombination life-

time is increased compared to the neutral bulk material. Indeed, as the photogenerated electrons and holes are spatially separated by the electric field, which is confined to the space-charge region, both the radiative and nonradiative recombinations are suppressed due to the lack of the opposite charges. The effect of electron-hole separation on the recombination time is further confirmed by the SPCM images of device C [Fig. 4(c)], as the spatial extension of the photocurrent profile under the forward bias condition (open circles and squares), which resembles the Ohmic device operation condition, is much larger than that of the photocurrent profile under the reversed bias condition (solid circles and squares), which is similar to the Schottky-barrier device operation condition. Spatially separated carrier transport is relevant to the operation of many devices including light-emitting devices and hybrid organic-inorganic photovoltaic devices, and the measurement of the figures of merit such as $\mu\tau$ provides a quantitative basis for device optimization and development efforts.

Finally, we would like to comment on the validity of the hypothesis that, under local optical excitation, the electric field, and therefore the potential drop, is primarily confined to the space-charge region in these intrinsic but Ohmically contacted devices. Following this hypothesis, the magnitude of the electric field is the voltage divided by the spatial extent of the space-charge region and does not depend on the device channel length. As a result, the fractional shift of the photocurrent peak, which depends on the magnitude of the electric field and the difference in the electron and hole mobilities,[14] should not vary between devices with different channel lengths. Indeed, the fractional shift of the photocurrent peak versus applied voltage is the same for two devices (B1 and B2) that were fabricated on the same nanowire, but with different channel lengths [Fig. 5(a)]. Since the magnitude of the electric field is proportional to the bias, this observation is consistent with our hypothesis. In contrast, if the electric field was well described by V_{bias}/L, where L is the device channel length, one then would expect that the fractional shift of the photocurrent peak as a function of V_{bias}/L for devices B1 and B2 would overlap, but this is clearly not the case in Fig. 5(b). Further support of this hypothesis will require comprehensive modeling of the carrier distribution

and internal potential; nevertheless, the qualitative observations presented here are consistent with our hypothesis.

V. SUMMARY

We have developed metal-nanowire contact fabrication procedures that consistently result in the controlled formation of Ohmic or Schottky contacts to CdS nanowires. SPCM images were found to be very sensitive to the nature of the contacts, and quantitative analysis of photocurrent profiles lead to the identification of dominant carrier transport processes and determination of the mobility-lifetime products of electrons and holes. In future studies, SPCM could help accelerate the development of nanowire-based devices by, for example, quantifying the effects of nanowire surface passivation to improve charge transport/collection efficiency. Complementary theoretical modeling of the carrier transport process in nanowires is needed to fully realize the potential of SPCM as a quantitative characterization method.

[1] R. Martel *et al.* Appl. Phys. Lett. **73**, 2447 (1998).
[2] K. Balasubramanian *et al.*, Appl. Phys. Lett. **84**, 2400 (2004); Y. Ahn, J. Dunning, and J. Park, Nano Lett. **5**, 1367 (2005).
[3] Y. Gu *et al.*, Appl. Phys. Lett. **87**, 043111 (2005).
[4] F. Galluzzi, J. Phys. D **18**, 685 (1985).
[5] D. Caputo, G. de Cesare, and M. Tucci, Sens. Actuators, A **88**, 139 (2001).
[6] N. Beck *et al.*, J. Appl. Phys. **79**, 9361 (1996).
[7] S. M. Sze, *Physics of Semiconductor Devices*, 2nd ed. (Wiley, New York, 1981).
[8] J. B. D. Soole and H. Schumacher, IEEE J. Quantum Electron. **27**, 737 (1991).
[9] F. A. Kroger, G. Diemer, and H. A. Klasens, Phys. Rev. **103**, 279 (1956).
[10] D. C. Look, J. Appl. Phys. **45**, 492 (1974).
[11] Under high-injection level condition ($\Delta n \gg n_0$, where Δn and n_0 are the concentration of photogenerated and thermal-equilibrium carrier concentration, respectively), a space-charge region forms at the point of optical injection, and this reduces the electric field outside the space-charge region, i.e., most of the external bias drops across the space-charge region. As a result, photogenerated carriers are separated inside the space-charge region via drift and diffusion process and subsequently diffuse towards the corresponding electrode. A description of the electric field distribution inside the space-charge region will require significant theoretical modeling beyond the scope of this presentation. See also Y. Gu, J. P. Romankiewicz, J. K. David, J. L. Lensch, and L. J. Lauhon, Nano Lett. **6**, 948 (2006).
[12] C. Weber *et al.*, Z. Phys. B: Condens. Matter **72**, 379 (1988).
[13] R. B. Stephens, Phys. Rev. B **29**, 3283 (1984).
[14] The difference in the electron and hole mobilities may vary as a function of electric field.